

# Kinetics and mechanism of the formation of silver nanoparticles by reduction of silver (I) with maltose in the presence of some active surfactants in aqueous medium

Hassan A. Ewais

Received: 6 March 2014 / Accepted: 19 March 2014 / Published online: 6 April 2014  
© Springer International Publishing Switzerland 2014

**Abstract** The kinetics and mechanism of the formation of silver nanoparticles by reduction of  $\text{Ag}^+$  with maltose were studied spectrophotometrically by monitoring the absorbance change at 412 nm in aqueous and micellar media at a temperature range 45–60 °C. The reaction was carried out under pseudo-first-order conditions by taking the [maltose] (>tenfold) the  $[\text{Ag}^+]$ . A mechanism of the reaction between silver ion and maltose is proposed, and the rate equation derived from the mechanism was consistent with the experimental rate law. The effect of surfactants, namely cetyltrimethylammonium bromide (CTAB, a cationic surfactant) and sodium dodecyl sulfate (SDS, an anionic surfactant), on the reaction rate has been studied. The enthalpy and the entropy of the activation were calculated using the transition state theory equation. The particle size of silver sols was characterized by transmission electron microscopy and some physicochemical and spectroscopic tools.

## Introduction

Silver nanoparticles have many applications in biotechnology [1], medicine [2], antibacterial agents [3], biosensors [4], catalysis and biochemical studies [5]. The evolution and technological progress of silver nanoparticles in the manufacture are due to their antiviral and antibacterial properties, in addition to numerous industrial applications including microelectronics,

cosmetics, adhesives and catalysis to enhanced solar cells [6–8]. The formation of nanoparticles using biological entities has great importance due to their individual shape-dependent optical, electrical and chemical properties, which have potential application in biotechnology [1].

The silver nanoparticles have been formed and stabilized by chemical and physical methods; chemical methods such as, electrochemical techniques, chemical reduction and photochemical reduction have been most widely used [9, 10]. The chemical reduction is the most used method for the formation of silver nanoparticles as stable, colloidal dispersions in aqueous or nonaqueous media [11, 12]. Hydrazine, aniline, ascorbic acid, glucose, lactose and sodium borohydride are used as reducing agents in the formation of nanoparticles [13–17]. Stabilizing agents such as cetyltrimethylammonium bromide, sodiumdodecyl sulfate, Tritron X-100 and poly (vinyl alcohol) are used as capping agents to control the shape and size of silver nanocrystals [13, 16, 18]. The reduction of silver ions ( $\text{Ag}^+$ ) in aqueous medium gave a colloidal silver with particle diameters of several nanometers [19]. The reduction of various complexes with  $\text{Ag}^+$  ions leads to the formation of silver atoms ( $\text{Ag}^0$ ), which is followed by agglomeration into oligomeric clusters [20]. These clusters eventually lead to the formation of colloidal Ag particles, which in solution have a yellow color [20].

In this work, the kinetics and mechanism of the formation of silver nanoparticles by reduction were studied in order to obtain a stable form of silver nanoparticles in aqueous and micellar media.

## Experimental

Silver nitrate, maltose, cetyltrimethylammonium bromide, sodium hydroxide, sodium dodecyl sulfate and potassium

H. A. Ewais (✉)  
Chemistry Department, Faculty of Science, King Abdulaziz  
University, P.O. Box 80203, Jeddah 21413, Saudi Arabia  
e-mail: hshalby2002@yahoo.com

H. A. Ewais  
Chemistry Department, Faculty of Science, Beni-Suef  
University, Beni Suef, Egypt

permanganate (Fluka and BDH) were used without further purification. The solutions of silver nitrate and maltose were prepared daily (to arrest the aerial oxidation) in boiled and cooled water. Doubly distilled water was used for the preparation of all solutions.

A UV–visible LABOMED, INC UVD-2960 spectrophotometer and PerkinElmer EZ-150 recording spectrophotometer were used to monitor the absorbance of the formation of silver sols. TEM images for the determination of the size of silver particles were recorded using a transmission electron microscope (JEOL, JEM-1011, Japan). The preparation of samples was carried out by adding a drop of working solution on a carbon-coated standard copper grid (300 mesh) operating at 80 kV. The Fourier transform infrared (FT-IR) spectra were investigated on a Bruker Equinox 55 spectrophotometer. A few drops of the silver sol were added on potassium bromide pellets, left to dry, and IR spectra recorded. The particles were imaged by LEO 440i Scanning Electron Microscopy (SEM) at an accelerating voltage of 20 kV. Elemental analysis of synthesized silver nanoparticles was recorded using an Energy Dispersive Spectrometer (EDS) JSM-7600F.

The UV–visible absorption spectra of the products (silver sol) were followed spectrophotometrically for a definite period of time using a LABOMED, INC UVD-2960 spectrophotometer. All reactants were equilibrated at the required temperatures in a thermostated water bath for ca. 15 min before being thoroughly mixed and quickly transferred to an absorption cell. The reaction rates were measured by monitoring the absorbance of product at 412 nm, on a PerkinElmer EZ-150 spectrophotometer, where the absorption of the products is maximal. The temperature of the reacting solution was adjusted, using an automatic circulation thermostat. The thermostat was provided with a special pumping system for circulating water at regulated temperature in the cell holder.

Pseudo-first-order conditions were maintained in all runs by the presence of a large excess (>tenfold) of maltose. Pseudo-first-order rate constants,  $k_{\text{obs}}$ , were obtained from the slopes of plots of  $\ln a/(1-a)$  versus time with a fixed-time method where  $a = A_t/A_\infty$  and  $A_t$  and  $A_\infty$  are the absorbencies at times and infinity, respectively [21]. Thermodynamic activation parameters  $\Delta H^*$  and  $\Delta S^*$  were calculated by plotting  $\ln(k/T)$  against  $1/T$  using the Eyring equation:

$$\ln k/T = \ln K/h + \Delta S^*/R - \Delta H^*/RT$$

where  $k$  the rate constant,  $K$  the Boltzmann constant,  $h$  Planck's constant,  $R$  universal gas constant and  $T$  absolute temperature.

The preparation of silver nanoparticles by the reduction of silver nitrate solution with maltose in the presence of

micelles in aqueous medium was investigated. A series of runs were carried out, using different concentrations of maltose, silver nitrate and CTAB to obtain a perfectly clear silver sol. In a similar procedure, 2.0 ml of a  $0.001 \text{ mol dm}^{-3}$  solution of silver nitrate and 4.0 ml of a  $0.1 \text{ mol dm}^{-3}$  sodium hydroxide solution were mixed with 4.0 ml of a  $0.01 \text{ mol dm}^{-3}$  CTAB solution. The pale yellow color of the silver sol was formed, when 2.0 ml of a  $0.02 \text{ mol dm}^{-3}$  solution of maltose was added to the reaction mixture at the beginning of reaction. The total volume of the reaction mixture was always 40 ml. The presence a pale yellow color indicated the formation of Ag nanoparticles [22, 23].

The solid sample of silver nanoparticles for FT-IR, EDS and SEM analysis was synthesized using the CTAB as stabilizer for silver nanoparticles that were formed from the aqueous colloidal solution via centrifugation by adding acetone as anti-solvent for several times, then drying.

## Results and discussion

### Formation and characterization of silver nanoparticles

The formation of silver nanoparticles using a suitable reducing agent and stabilizer for the stability of Ag nanoparticles is very important because the shape and size depend on the nature of stabilizers and reducing agent [23]. Metal nanoparticles synthesized by means of moderate reducing agents were comparatively more stable than those produced by strong reducing agents [24]. Maltose is one of the relatively moderate reducing agents used for the reduction of silver ions in the presence of CTAB as stabilizer.

UV–visible absorption spectra have proven to be sensitive to the formation of silver sols because silver nanoparticles show a strong absorption peak due to the surface plasmon excitation. Spectra of the product were recorded between the wavelength range from 300 to 600 nm as a function of time (Fig. 1). The maximum absorption was obtained at wavelength 412 nm, showing the formation of Ag nanoparticles. This indicates that the absorbance increases at 412 nm with time. The absorption plasmon band with a  $\lambda_{\text{max}}$  at 412 nm is the characteristic of spherical or roughly spherical shape Ag-nanoparticles synthesis.

FT-IR is tool to characterize the state of silver nanoparticles present in the colloidal solution. IR was used for a qualitative investigation, to see if CTAB-capped silver nanoparticles would have different IR spectra. The bands at  $3,291$  and  $1,629 \text{ cm}^{-1}$  are broad and sharp and assigned to the hydroxyl groups from adsorbed moisture. These bands are absent from the silver nitrate and CTAB spectra. The

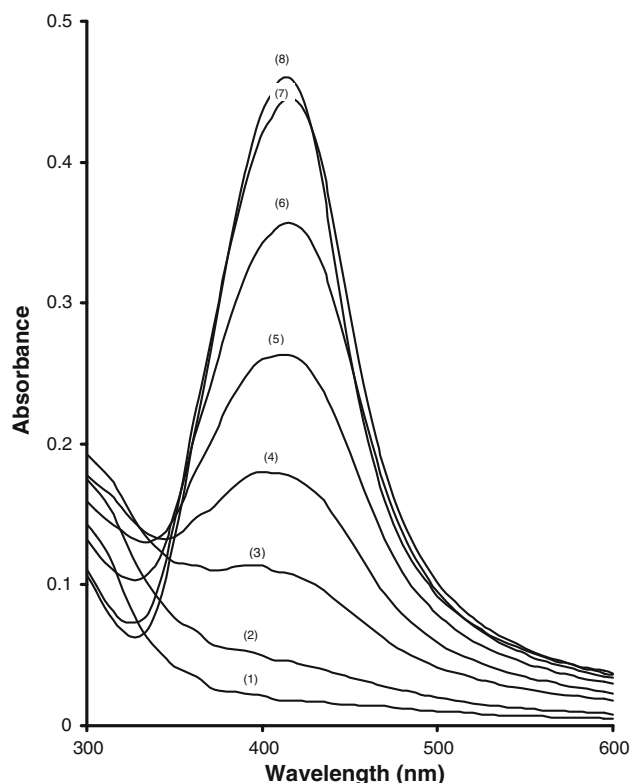


**Fig. 1** Absorbance spectra of reaction mixtures versus time. Curves (1–8) were recorded at 2, 5, 10, 15, 20, 30, 42 and 50 min. at  $[Ag^+] = 5.0 \times 10^{-5} \text{ mol dm}^{-3}$ ,  $[\text{maltose}] = 1.0 \times 10^{-3} \text{ mol dm}^{-3}$ ,  $[\text{CTAB}] = 1.0 \times 10^{-3} \text{ mol dm}^{-3}$ ,  $[\text{NaOH}] = 10 \times 10^{-3} \text{ mol dm}^{-3}$  and  $T = 50 \text{ }^\circ\text{C}$

observed bands of CTAB appear at 2,910, 2,844, 1,431, 955, 902 and  $714 \text{ cm}^{-1}$ . This may be attributed to the constraints imposed on chemical bond vibrations in CTAB molecules being the same as those of CTAB-capped silver nanoparticles.

EDS was used to measure the chemical composition and crystal structure of the silver nanoparticles. Figure 2 shows the EDS spectrum where the peaks at 3.2 and 3.5 keV correspond to silver, while those at 0.2 and 0.4 keV correspond to carbon and oxygen. The lower intensity peaks at 0.5, 1.0 and 1.5 keV belong to copper, zinc and bromide, respectively. Copper and zinc appeared because of the copper grid used to deposit the nanoparticles for their EDS characterization. Carbon, oxygen and bromide are due to CTAB adsorbed on the nanoparticles. These results confirmed that the nanoparticles being synthesized are silver. Figure 3 shows the SEM images of silver nanoparticles were prepared and measured as a solid sample (Fig. 3a) or solution sample (Fig. 3b). From the SEM images, it is observed that the particles had a relatively narrow size and a spherical shape. The size of silver nanoparticle ranges from 14.84 to 36.44 nm and the shapes are variable, being spherical and irregular with broad size distribution (Fig. 3b). A TEM image of the prepared Ag nanoparticles is represented as shown in Fig. 4. From Fig. 4, it clear

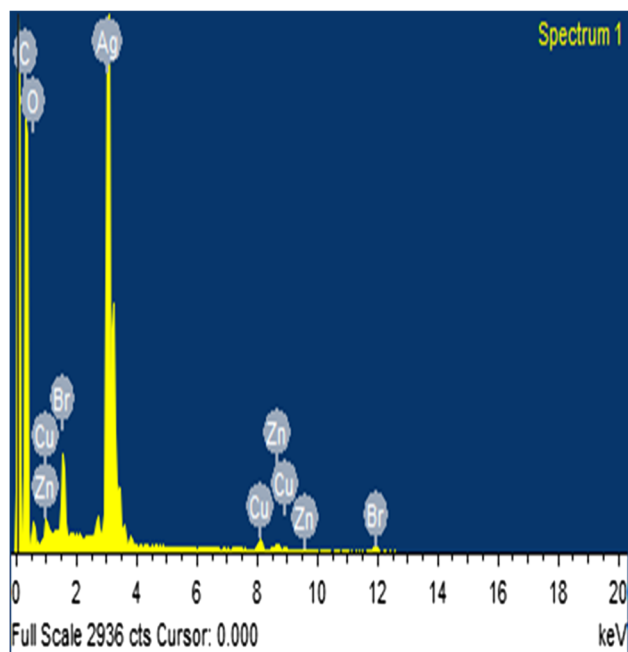


**Fig. 2** EDS of the silver nanoparticles was confirmed the presence of elemental silver signal

that the size of the nearly spherical nanoparticles ranges between 13.12 and 39.23 nm and their size distribution is relatively wide. The TEM micrograph confirms the formation of CTAB stabilized spherical Ag nanoparticles rather than hexagonal close-packed arrays and nanorods of Ag nanocrystals as observed in the reduction in  $Ag^+$  ions with hydrazine and glucose, respectively [25, 26].

#### Kinetics of formation of silver nanoparticles

The kinetics of the formation of Ag nanoparticles by reduction with maltose were studied at different concentrations of  $Ag^+$ , maltose, NaOH and CTAB over a temperature range (45–60)  $^\circ\text{C}$ . Plotting absorbance versus time (Fig. 5) shows both a non-catalytic and autocatalytic reaction path. The observation of autocatalysis in Fig. 5 is due to the formation of metal nucleation centers that act as a catalyst for the reduction of other silver ions present in solution. Figure 6 suggests that autocatalysis is involved in the silver sol formation. In the present study, it is necessary to point out that the plots of  $\ln a/(1-a)$  against time are linear up to >85 % of the reaction (Fig. 6), where  $a = A_t/A_\infty$  and  $A_t$  and  $A_\infty$  are the absorbances at times  $t$  and infinity  $\infty$ , respectively [21]. The values of the rate constants were obtained from the slopes of  $\ln a/(1-a)$  versus time plots (Table 1). The constancy of  $k_{\text{obs}}$  over the  $[Ag^+]$  range  $(2.50\text{--}7.50) \times 10^{-5} \text{ mol dm}^{-3}$  at constant maltose concentration indicates first order dependence on the  $[Ag^+]$  as shown in Table 1 and Eq. (1)

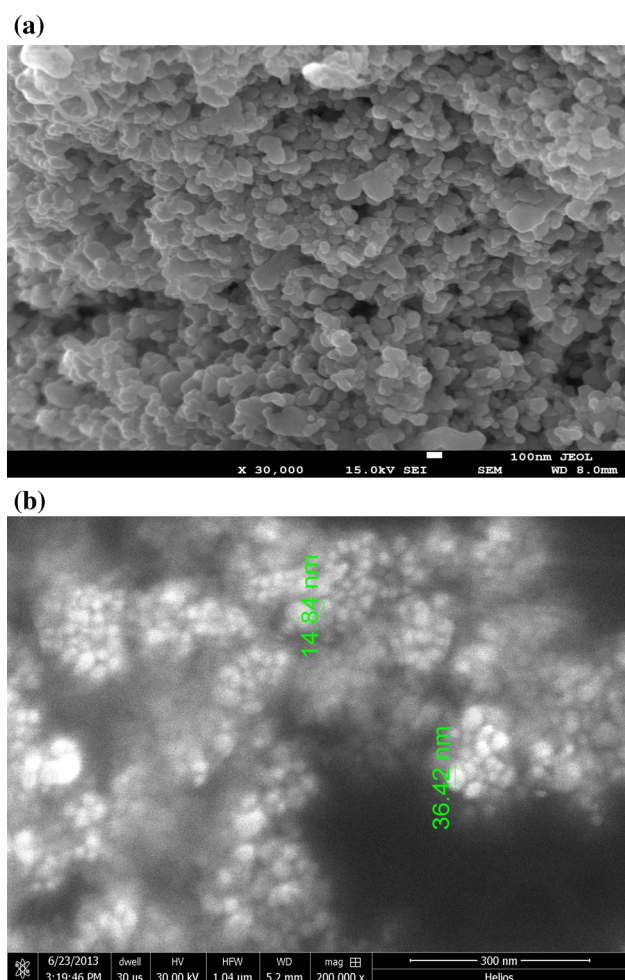


**Fig. 3** SEM images of silver nanoparticles that were obtained as the final products under the optimal conditions mentioned under Fig. 1. **a** Solid sample. **b** Solution sample

$$\text{Rate} = k_{\text{obs}}[\text{Ag}^+]. \quad (1)$$

The dependence of the observed rate constant,  $k_{\text{obs}}$ , on maltose (R-CHO) was studied over the concentration range  $(0.5\text{--}2.0) \times 10^{-3} \text{ mol dm}^{-3}$  at fixed  $[\text{Ag}^+]$  ( $=5.0 \times 10^{-5} \text{ mol dm}^{-3}$ ),  $[\text{NaOH}]$  ( $=10 \times 10^{-3}$ ) and  $[\text{CTAB}]$  ( $=1.0 \times 10^{-3}$ ) at  $T = 50^\circ\text{C}$ . The results in Table 1 and Fig. 7 show that  $k_{\text{obs}}$  varies linearly with [R-CHO] according to Eq. (2):

$$k_{\text{obs}} = k_1[\text{R-CHO}]. \quad (2)$$

The kinetics of the formation of silver nanoparticles were studied over a  $[\text{NaOH}]$  range of  $(2.50\text{--}15.0) \times 10^{-3} \text{ mol dm}^{-3}$  at different temperatures. The values of  $k_1$  with  $[\text{NaOH}]$  at different temperatures are represented in Table 2 and shows that the rate increased gradually with increasing  $[\text{NaOH}]$ . Plots of the slope  $k_1$  against  $[\text{OH}^-]$  were linear, with intercepts as shown in Fig. 8. It can be seen that this variation is described by Eq. (3):

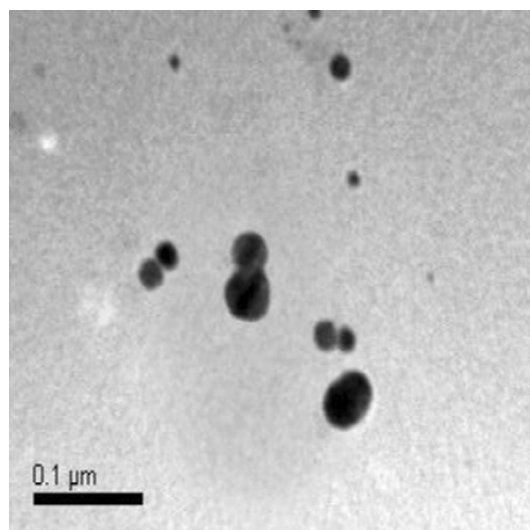


**Fig. 4** TEM images of silver nanoparticles that were obtained as the final products under the optimal conditions mentioned under Fig. 1

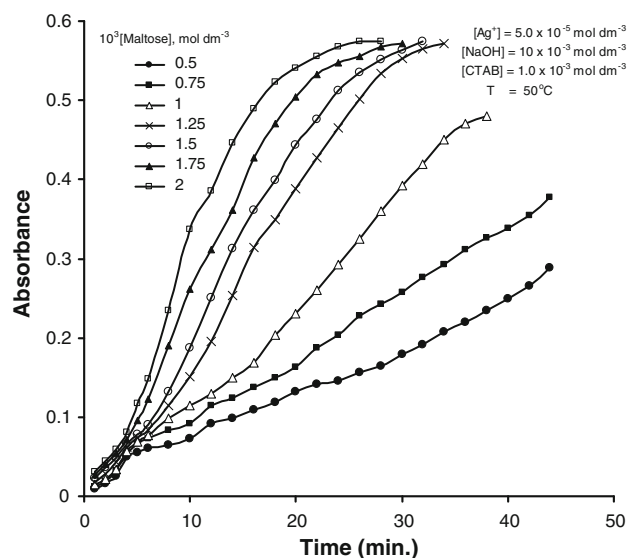


**Fig. 5** Absorbance–time curves of silver sol formation at different [maltose]

$$k_1 = k_2 + k_3[\text{OH}^-] \quad (3)$$

From Eqs (1), (2) and (3) the rate law for the reduction in  $[\text{Ag}^+]$  by maltose is given by Eq. (4):

$$\text{Rate} = (k_2 + k_3[\text{OH}^-])[\text{Ag}^+][\text{R-CHO}] \quad (4)$$

and

$$k_{\text{obs}} = [\text{R-CHO}](k_2 + k_3[\text{OH}^-]). \quad (5)$$

The  $k_2$  and  $k_3$  values, collected in Table 3 at the temperatures used were gained from the intercepts and the



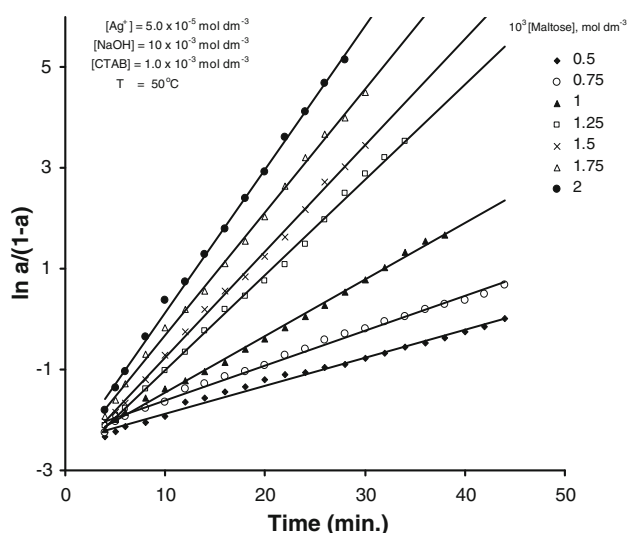


**Fig. 6** Plots of  $\ln a/(1-a)$  versus time at different [maltose]

**Table 1** Dependence of the  $[Ag^+]/[maltose]$  reaction rate on  $[Ag^+]$ ,  $[maltose]$  and  $[CTAB] = 1.0 \times 10^{-3} \text{ mol dm}^{-3}$  at  $T = 50.0 \text{ }^\circ\text{C}$

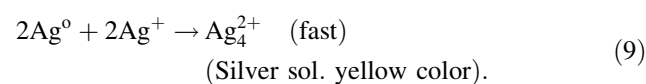
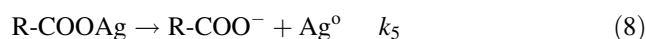
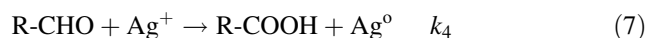
$10^3 [OH^-]$ $\text{mol dm}^{-3}$	$10^5 [Ag^+]$ $\text{mol dm}^{-3}$	$10^3 [maltose]$ $\text{mol dm}^{-3}$	$10^3 k_{obs} \text{ s}^{-1}$
10.00	5.00	2.00	4.58
		1.75	4.08
		1.50	3.58
		1.25	3.13
		1.00	2.35
		0.75	1.63
		0.50	1.14
		2.50	1.00
5.00	10.00	1.00	1.38
		1.00	1.97
		1.00	2.55
		1.00	2.98
		2.50	2.19
		3.75	2.47
		5.00	2.35
		6.25	2.66
7.50	10.00	1.00	2.54

slopes, respectively, of Fig. 8. The enthalpy of activation  $\Delta H_2^*$  and  $\Delta H_3^*$  related to  $k_2$  and  $k_3$  were obtained from the Eyring equation as 25.2 and 37.4  $\text{kJ mol}^{-1}$ , respectively. The corresponding entropies of activation  $\Delta S_2^*$  and  $\Delta S_3^*$  were calculated as  $-169.8$  and  $-68 \text{ JK}^{-1} \text{ mol}^{-1}$ , respectively.

### Mechanism

The formation of silver sol in aqueous medium involves different species of silver metal particles. Several species

of silver ions like  $Ag_2^+$ ,  $Ag_4^{2+}$ ,  $Ag_3^+$ ,  $Ag_6^{4+}$  and  $Ag_9^+$  exist in aqueous medium [27, 28], as suggested by Henglein et al. [27] and other researchers [28].  $Ag_4^{2+}$  is the more stable species for a long time in the presence of active surfactants. Equation (6) involved a complex formation between R-CHO and  $Ag^+$  in alkaline medium. In the rate-determining step, the complex, R-COOAg, decomposes unimolecularly through a one electron oxidation–reduction mechanism to the formation of  $Ag^0$  (Eq. (8)). In the following step,  $Ag^0$  reacts with  $Ag^+$  to yield a silver sol ( $Ag_4^{2+}$ ) (Eq. (9)) [27]. The suggested mechanism is described by Eqs. (6–9):



From the above mechanism the rate law is given by:

$$\text{Rate} = k_4[R-CHO][Ag^+] + k_5[R-COOAg]. \quad (10)$$

From Equilibrium (6), we obtained:

$$R-COOAg = K_1[R-CHO][Ag^+][OH^-]. \quad (11)$$

Substitution Eq. (11) in Eq. (10), gave Eq. (12).

$$\text{Rate} = k_4[R-CHO][Ag^+] + k_5K_1[R-CHO][Ag^+][OH^-] \quad (12)$$

$$\text{Rate} = [R-CHO][Ag^+](k_4 + k_5K_1[OH^-]) \quad (13)$$

and

$$k_{obs} = [R-CHO](k_4 + k_5K_1[OH^-]). \quad (14)$$

Comparing Eqs. (14) and (5), one obtained  $k_2 = k_4$  and  $k_3 = k_1k_5$ . Eq. (14) contains two terms; the first term represents the path independent of  $[OH^-]$  and the second term represents the path dependent on  $[OH^-]$ .

In comparison with the formation of silver nanoparticles by reduction with glucose [26] under the same conditions, the rate-determining step is via one electron oxidation–reduction mechanism in both cases. The rate of formation of silver nanoparticles by the reduction with maltose is lower than the rate of formation by reduction with glucose. This may be because maltose as a reducing sugar has only half the reduction ability per unit mass.

### Effect of micelles on the rate of formation of silver nanoparticles

Micellar catalysis has received considerable attention in view of the analogies drawn between micellar and enzyme catalyses [29, 30]. Micelles increase rates of bimolecular reactions

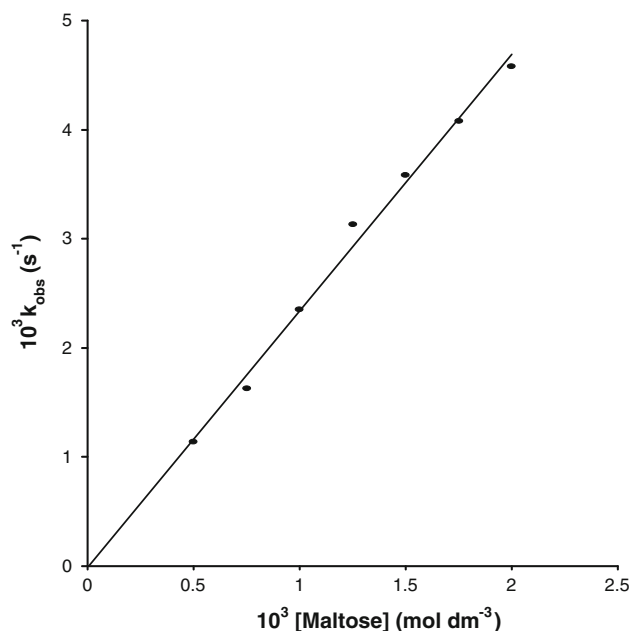


**Fig. 7** Plot of  $k_{\text{obs}}$  versus [maltose] at 50 °C

**Table 2** Variation in  $k_1$  with hydroxide ion concentration at  $[\text{Ag}^+] = 5.0 \times 10^{-5} \text{ mol dm}^{-3}$ , [maltose] =  $1.0 \times 10^{-3} \text{ mol dm}^{-3}$  [CTAB] =  $1.0 \times 10^{-3} \text{ mol dm}^{-3}$  and at different temperatures

$10^3[\text{OH}^-] \text{ mol dm}^{-3}$	$k_1 \text{ dm}^3 \text{ mol}^{-1} \text{ s}^{-1}$			
	$T = 45.0 \text{ }^\circ\text{C}$	$50.0 \text{ }^\circ\text{C}$	$55.0 \text{ }^\circ\text{C}$	$60.0 \text{ }^\circ\text{C}$
2.50	0.72	1.11	1.49	1.63
5.00	0.95	1.38	1.84	2.07
7.50	1.33	1.97	2.48	2.81
10.00	1.66	2.35	2.91	3.54
12.50	2.06	2.55	3.62	4.13
15.00	2.25	2.98	4.04	4.60

by concentrating both the reactants at their surfaces. Electrostatic, approximation, and medium-effects are responsible for the incorporation of reactants into or onto a micelle. In order to verify the role of micelles on the formation of silver nanoparticles by reduction with maltose, cationic and anionic micelles were chosen. The effect of micelles (CTAB and SDS) on the formation of silver nanoparticle by reduction with maltose was carried at  $[\text{Ag}^+] = 5.0 \times 10^{-5} \text{ mol dm}^{-3}$ , [maltose] =  $1.0 \times 10^{-3} \text{ mol dm}^{-3}$ ,  $[\text{OH}^-] = 10 \times 10^{-3} \text{ mol dm}^{-3}$ , [CTAB] = [SDS] =  $1.0 \times 10^{-3} \text{ mol dm}^{-3}$  and  $T = 50.0 \text{ }^\circ\text{C}$ . Figure 9 plots of maximum wavelength absorbance *versus* time clearly indicate that the absorbance associated with formation of silver nanoparticles gradually increases with time in presence of CTAB, but a rapid increase in absorbance of silver sol at the beginning of the reaction is observed in the presence of SDS.

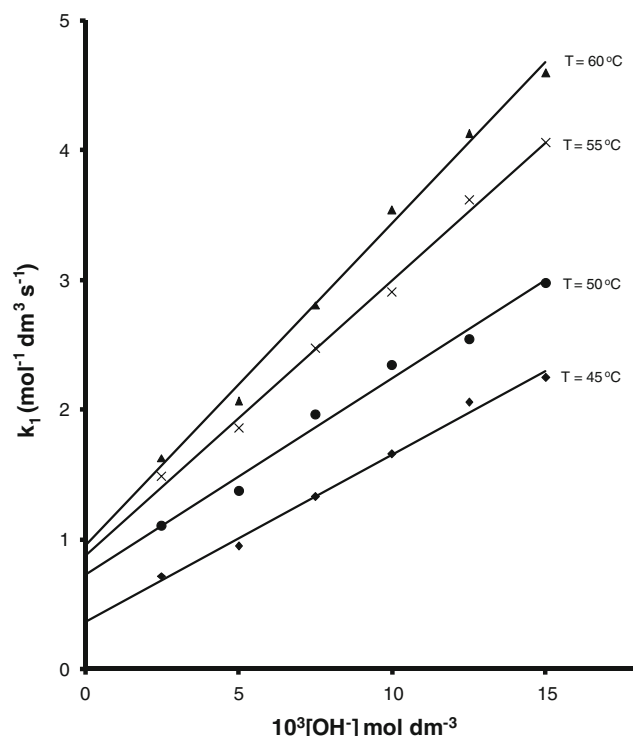


**Fig. 8** Plot of  $k_1$  versus  $[\text{OH}^-]$  at different temperatures

**Table 3** Variation in hydroxide-independent rate constant  $k_2$  and hydroxide dependent rate constant  $k_3$  with temperature

Temp. $^\circ\text{C}$	$10 k_2 \text{ dm}^3 \text{ mol}^{-1} \text{ s}^{-1}$	$10^{-2} k_3 \text{ dm}^6 \text{ mol}^{-2} \text{ s}^{-1}$
45.0	3.64	1.30
50.0	7.34	1.51
55.0	8.81	2.12
60.0	9.54	2.49

The role of micelles in catalysis and inhibition of some reactions is due to the solubilization and/or incorporation of reactants into the small volume of micelles through electrostatic, hydrophobic, hydrogen bonding and van der Waals forces [30] and [31]. The different behavior of SDS and CTAB micelles in the formation of silver sol due to the presence of positive charge on the  $\text{Ag}^+$  and its metal particles in the reaction medium. The formation of ion pairs ( $-\text{OSO}_3^- \text{Ag}^+$ ) from the positive charge on  $\text{Ag}^+$  with the negative head group of SDS micelles which concentrate the  $\text{Ag}^+$  through the electrostatic interactions into the reaction site (i.e., Stern layer as most of the ionic micelle mediated reactions are believed to occur in this region). Furthermore, electrostatic repulsion between the positive head group ( $-\text{N}^+(\text{CH}_3)_3$ ) of CTAB micelles with silver ion  $\text{Ag}^+$  is present in the bulk aqueous pseudo-phases. According to the following observations, the reaction proceeds faster in the presence of SDS than that of CTAB.

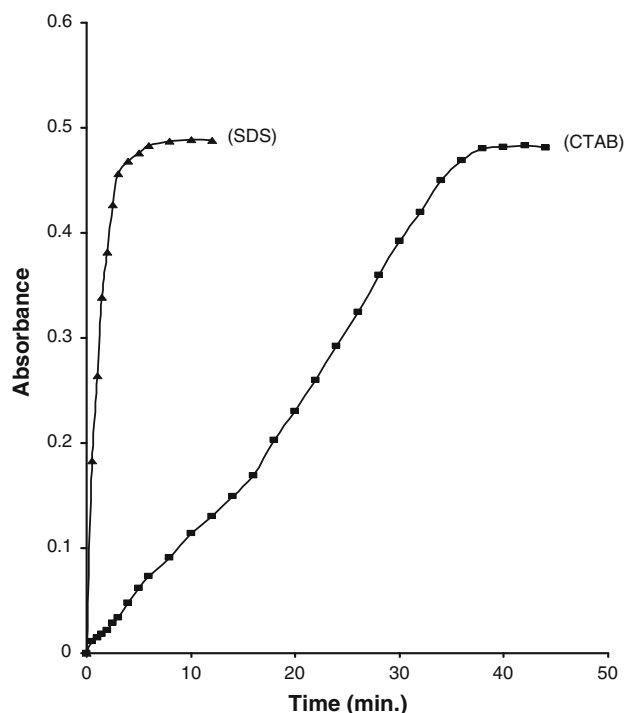


**Fig. 9** Absorbance versus time plots for silver nanoparticles formation in presence of CTAB and SDS. *Reaction conditions:*  $[Ag^+] = 5.0 \times 10^{-5} \text{ mol dm}^{-3}$ ,  $[\text{maltose}] = 1.0 \times 10^{-3} \text{ mol dm}^{-3}$ ,  $[\text{SDS}] = [\text{CTAB}] = 1.0 \times 10^{-3} \text{ mol dm}^{-3}$ ,  $[\text{OH}^-] = 10 \times 10^{-3} \text{ mol dm}^{-3}$  and  $T = 50 \text{ }^\circ\text{C}$

The negative values of the entropies of activation for this reaction may result from the charge concentration of the reactants, which causes substantial mutual ordering of the solvated water molecules [32]. The intermolecular electron transfer steps are endothermic as indicated by the positive  $\Delta H^*$  values. The contributions of  $\Delta H^*$  and  $\Delta S^*$  to the reaction rate seem to compensate each other. This suggests that the factors affecting  $\Delta H^*$  should be closely related to those controlling  $\Delta S^*$ .

## Conclusions

The results from this study show that the reduction in silver(I) by maltose is enhanced in the presence of NaOH, leading to the formation of stable and transparent yellow colored silver sol. The kinetics of silver sol formation were monitored by recording the absorbance as a function of time. The rate of formation of silver nanoparticles gradually increases with time in presence of CTAB, but rapidly increases at the beginning of the reaction in the presence of

SDS. The particle size of silver sol was characterized by UV-SP, Fit-IR, EDS, SEM and TEM.

**Acknowledgments** This work was funded by the Deanship of Scientific Research (DSR), King Abdulaziz University, Jeddah, under grant No. (130-010-D1433). The authors, therefore, acknowledge with thanks DSR technical and financial support.

## References

- Anil-Kumar S, Abyanesh MK, Gosavi SW, Kulkarni SK, Pasricha R, Ahmed M, Khan MI (2007) *Biotechnol Lett* 29:439
- Schultz DA (2003) *Curr Opin Biotech* 14:13
- Gopinath K, Gowri S, Arumugam A (2013) *J Nanost Chem* 3:68
- Nam JM, Thaxton CS, Mirkin CA (2003) *Science* 301:1884
- Haneda M, Kintaichi Y, Inaba M, Hamada H (1998) *Catal Today* 42:127
- Sharma VK, Yngard RA, Lin Y (2009) *Adv Colloid Interface Sci* 145:83
- Sotiriou GA, Pratsinis SE (2010) *Environ Sci Technol* 44:5649
- Wigginton NS, de Titta A, Piccapietra F, Dobias J, Nesatyy VJ, Suter MJF, Bernier-Latmani R (2010) *Environ Sci Technol* 44:2163
- Chen W, Cai W, Zhang L, Wang G (2001) *J Colloid Interface Sci* 238:291
- Frattoni A, Pellegrini N, Nicastro D, de Sanctis O (2005) *Mater Chem Phys* 94:148
- Patakfalvi R, Viranyi Z, Dekany I (2004) *Colloid Polym Sci* 283:299
- Kiim M, Byun JW, Shin DS, Lee YS (2009) *Mat Res Bull* 44:334
- Al-Thabati SA, Obaid AY, Al-Youbi AO (2009) *Colloid Surf B Biointerface* 73:284
- Khan Z, Al-Thabati SA, Obaid AY, Al-Youbi AO (2010) *Colloid Surf B Biointerface* 78:143
- Sahoo PK, Kalyan Kamal SS, Jagadeesh Kumar T, Sreedhar B, Singh AK, Srivastava SK (2010) *Def Sci* 59:447
- Khan Z, Al-Thabati SA, Obaid AY, Khan ZA, Al-Youbi AO (2012) *J Colloid Interface Sci* 367:101
- Linnert T, Mulvaney P, Henglein A (1990) *J Am Chem Soc* 112:4657
- Henglein A (1998) *Chem Mater* 10:444
- Wiley B, Sun Y, Mayers B (2005) *Chem Eur J* 11:454
- Kapoor S, Lawless D, Kennepohl P, Meisel D, Serpone N (1994) *Langmuir* 10:3018
- Esumi K, Hosoyo T, Yamahira A, Torigoe K (2000) *J Colloid Interface Sci* 226:346
- Sharma VK, Yngard RA, Lin Y (2009) *Adv Colloid Interface Sci* 145:83
- Henglein A (1993) *J Phys Chem* 97:5457
- Heinzman SW, Gamen B (1982) *J Am Chem Soc* 104:6801
- Tan Y, Li Y, Zhu D (2003) *J Colloid Interface Sci* 258:244
- El-Shishtawy RM, Asiri AM, Al-Otobi MM (2011) *Spectrochim Acta A* 79:1505
- Ershov BG, Janata E, Henglein A, Fojtik A (1993) *J Phys Chem* 97:4589
- Wasowicz T, Michalik R (1991) *J Phys Chem* 37:427
- Menger FM, Portony CE (1967) *J Am Chem Soc* 89:4698
- Bunton CA, Savelli G (1986) *Adv Phys Org Chem* 22:213
- Bunton CA (1997) *J Mol Liq* 72:231
- Weaver MJ, Yee EL (1980) *Inorg Chem* 19:1936